PERGAMON

Electrochimica Acta 44 (1998) 59–71

ELECTROCHIMICA Acta

Determination of rate constants of ion transfer kinetics across immiscible electrolyte solutions

José A. Manzanares [a,*], Riikka Lahtinen [b], Bernie Quinn [b], Kyösti Kontturi [b], David J. Schiffrin [c]

[a] *Department of Thermodynamics, University of Valencia, 46100 Burjassot, Spain*
[b] *Laboratory of Physical Chemistry and Electrochemistry, Helsinki University of Technology, P.O. Box 6100, 02015 HUT, Finland*
[c] *Department of Chemistry, University of Liverpool, P.O. Box 147, Liverpool L69 7M, UK*

Received 16 October 1997

Abstract

The rotating diffusion cell was used to study ion transfer across the interface between two immiscible electrolyte solutions. Tetrabutylammonium was chosen as the transferring cation and lithium chloride as the supporting electrolyte in aqueous phase. Tetrabutylammonium tetrakis-(4-fluorophenyl)-borate in 2-nitrophenyl-octylether was used as the organic electrolyte solution supported in the porous membrane. The quasi-steady state current–voltage curves were measured both by applying potential steps and by imposing a slow potential sweep. The analysis of experimental results was based on the comparison with the theoretical current–voltage curves and on the Koutecky–Levich plots. The apparent electrical resistance at low applied potentials was also considered. Some experimental limitations which make the rotating diffusion cell suitable only for a limited range of values of the standard rate constant to be determined were identified. In particular, it was shown that the method requires an accurate evaluation of the different contributions to the ion permeability. Nevertheless, an estimation of the rate constant for ion transfer in the system studied was obtained.

Keywords: ITIES; Rotating diffusion cell; Supported liquid membrane; Ion transfer; Rate constant

1. Introduction

Ion transfer across the interface between two immiscible electrolyte solutions (ITIES) is of great theoretical and practical interest. The rate constant can reflect the changes in the ionic solvation environment as the ion crosses from one phase to the other. There is a discussion on the fundamental aspects of this problem, i.e. whether an activated step is involved in the transfer process due to solvent reorientation or the whole transfer reaction can be analysed as an electrodiffusion problem through a dielectric discontinuity. Besides the theoretical importance of these questions, the application of ion transfer studies to practical problems, such as metal ion recycling or hydrometallurgy are well recognized.

However, measured values of the standard rate constant k^0 for transfer across the ITIES appear to depend strongly on the technique used [1, 2]. The techniques mostly used are based on ac impedance with different cell configurations. As pointed out previously [3], concentration polarization significantly affects ion transfer kinetics in the presence of electric current across the interface. Even though in many cases it is possible to arrange these experiments so that the current on a time-average basis is zero, this may be difficult when the solubility of the transferred ion in the organic phase is low. Therefore, methods where the mass transport (and therefore the interfacial concentrations) can be theoretically calculated are prefer-

* Corresponding author.

0013-4686/98/$19.00
PII: S0013-4686(98)00152-2

able. In the case of the ITIES, microholes [4, 5] and rotating diffusion cells [6] can be employed.

The rotating diffusion cell (RDC) has not been applied so far to the study of ion transfer kinetics across the ITIES. Because of the stationary nature of ion transfer in this case, the theoretical analysis becomes simpler and more reliable than for transient experiments. Furthermore, the RDC enables kinetic studies for non-zero electric current, which is important because the interfacial structure may be greatly dependent on ionic flux. The method, however, requires an accurate evaluation of the different contributions to the ion permeability, for the response of this system is determined by the transport across two aqueous solutions, the organic phase and the two interfaces, and the permeabilities of these regions are affected by the concentration polarization.

2. Theory

2.1. Rotating diffusion cell

Fig. 1 shows schematically the configuration of the RDC used. The principle employed in this work is that of electroassisted ion transfer for a reaction such as

$$TBA^+(w) \rightleftarrows TBA^+(o) \quad (1)$$

where TBA^+ is the tetrabutylammonium cation. The two phase equilibrium condition is given by

$$\Delta_o^w\phi_{eq} = \Delta_o^w\phi^0_{TBA^+} + \frac{RT}{F}\ln\frac{a^o_{TBA^+}}{a^w_{TBA^+}} \quad (2)$$

where ϕ is the Galvani potential, F the Faraday constant, R the gas constant, T the absolute temperature and a_i the ionic activities, which will be replaced by concentrations for the sake of simplicity. Superscripts o and w refer to the organic and aqueous phases, respectively. $\Delta_o^w\phi^0_{TBA^+}$ is the standard potential difference.

The equilibrium described in Eq. (2) can be altered by imposing externally an interfacial potential difference, forcing the system out of equilibrium. Thus, the transfer of TBA^+ from the aqueous to the organic phase can be *externally* induced by making $\Delta_o^w\phi$ more positive than $\Delta_o^w\phi_{eq}$. The opposite effects occur at the membrane/solution interface in the receiving phase. These are the basic principles involved in the electroassisted transfer of ions across a thin supported liquid membrane (SLM). In the present work, the mass transfer coefficient, which is important in determining the ionic flux, is established by the hydrodynamics of convective flow at a rotating supported membrane surface.

The cell to be considered is

	aqueous solution	organic solution	aqueous solution	
Ag/AgCl	c_sLiCl + c_tTBACl	c_mTBATPBF$_4$	c_sLiCl + c_tTBACl	AgCl/Ag

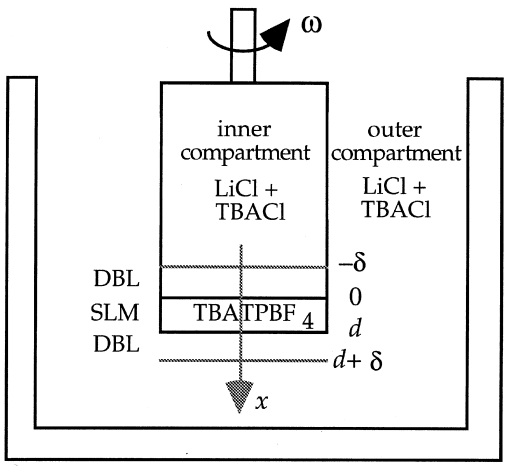

Fig. 1. Sketch of the RDC cell.

where $TPBF_4^-$ is the tetrakis-(4-fluorophenyl)borate anion. The current is transported by TBA^+, at a rate determined by mass transfer in the aqueous and organic phases and by kinetics at the boundaries. The system is modeled as one dimensional, with the SLM extending from $x = 0$ to $x = d$. The diffusion boundary layers (DBL) extend from $x = -\delta$ to $x = 0$ and from $x = d$ to $x = d + \delta$. The rotating disk geometry allows for a precise control of the thickness δ and hence, of the observed current. In particular, this thickness is given by the Levich equation [7]

$$\delta = 0.643(D^w_{TBA^+})^{1/3}\nu^{1/6}\omega^{-1/2} \quad (3)$$

where $D_{TBA^+}{}^w$ is the diffusion coefficient of TBA^+ in aqueous phase, ν is the aqueous solution viscosity (10^{-2} cm^2/s, in the case of dilute solution) and ω is the rotation frequency (in Hz).

The molar ion concentrations in the bulk of the

inner and outer compartments are

$$c_{TBA^+} = c_t, \qquad c_{Cl^-} = c_s + c_t, \qquad c_{Li^+} = c_s,$$
$$c_{TPBF_4^-} = 0 \quad \text{at } x = -\delta \text{ and } x = d + \delta. \tag{4}$$

In the SLM no supporting electrolyte is present ($c_{Cl^-} = c_{Li^+} = 0$) and the organic anion $TPBF_4^-$ is so hydrophobic that it remains in this phase for all applied currents. The average $TPBF_4^-$ concentration in the SLM

$$c_m = \frac{1}{d}\int_0^d c_{TPBF_4^-}\,dx \tag{5}$$

remains then constant while TBA^+ is transferring across the SLM. Ion pairing effects, which may appear because of the low dielectric constant of the organic solvents usually employed in ion transfer studies, can be accounted for multiplying c_m by the degree of dissociation.

2.2. Steady-state current–voltage characteristics

When a potential difference $\Delta\phi_{cell}$ is applied to the RDC cell, it distributes in the bulk and interfacial regions as given by

$$\Delta\phi_{cell} = \Delta\phi_I + \Delta_w^o\phi(0) + \Delta\phi_M + \Delta_o^w\phi(d) + \Delta\phi_O \tag{6}$$

where subscripts I, M and O stand for inner DBL, SLM and outer DBL, respectively. $\Delta\phi$ denotes the Galvani potential drop across the corresponding region or interface. These potential drops are evaluated by solving the Nernst–Planck equations in the DBLs and in the SLM and coupling the solutions obtained with the Butler–Volmer equations for the DBL/SLM interfaces at $x = 0$ and $x = d$. The potential drops at the interfaces are the sum of the Nernst potentials and the overpotentials. The Nernstian potential differences are responsible for the typical shape of the current–voltage curves, since they diverge when the transferring ion concentration approaches zero in the aqueous phase. The magnitude of the overpotentials represents the importance of the kinetic limitations at the interfaces and it affects the shape of the current–voltage curves, thus enabling to determine the standard rate constant for ion transfer. In what follows, the transport conditions in the DBLs and the SLM are analysed separately.

2.2.1. Aqueous phase

The Nernst–Planck equation

$$J_i = -D_i^\varphi\left(\frac{dc_i}{dx} + z_i f c_i \frac{d\phi}{dx}\right) \tag{7}$$

displays the flux density of species i as the sum of diffusional and migrational contributions. In Eq. (7), D_i^φ and z_i are the diffusion coefficient in phase φ and the charge number of ionic species i, respectively, and $f = F/RT$. The flux density of the transferred ion is

$$J_{TBA^+} = I/FA \tag{8}$$

where A is the effective membrane area and all other ionic flux densities J_i are zero.

Due to the presence of the supporting electrolyte, the potential drop in the DBLs is often negligible and the TBA^+ transport takes place mostly by diffusion

$$J_{TBA^+} \approx -D_{TBA^+}^w \frac{dc_{TBA^+}}{dx}. \tag{9}$$

Since J_{TBA^+} is constant, the concentration profile of TBA^+ is approximately linear and varies from c_t at $x = -\delta$ to

$$c_{TBA^+}^w(0) \approx c_t(1 - I/I_L) \tag{10a}$$

in the inner DBL and from

$$c_{TBA^+}^w(d) \approx c_t(1 + I/I_L) \tag{10b}$$

to c_t at $x = d + \delta$ in the outer DBL. In Eqs. (10a)–(b),

$$I_L = FAD_{TBA^+}^w c_t/\delta \tag{11}$$

is the limiting current for the transferring ion in the DBL. When the transferring ion concentration in the aqueous solutions is not so small, $c_t \lesssim c_s$, a more rigorous analysis is required (Appendix A).

2.2.2. Organic phase

Since the $TPBF_4^-$ ion is not transferring across the SLM, the diffusional and migrational terms in the Nernst–Planck equation for this ion must cancel out each other. The local electroneutrality condition ($c_{TBA^+} = c_{TPBF_4^-}$) implies then that the diffusional and migrational terms in the flux equation for TBA^+ are equal to each other, and therefore the concentration profile of TBA^+ is linear. Furthermore, taking into account that the average concentration of TBA^+ (and $TPBF_4^-$) inside the SLM is c_m (see Eq. (5)) it is easily obtained that

$$c_{TBA^+}^o(0) = c_m(1 + I/I_{LM}), \tag{12a}$$

$$c_{TBA^+}^o(d) = c_m(1 - I/I_{LM}), \tag{12b}$$

where

$$I_{LM} \equiv 4FAD_{TBA^+}^o c_m/d \tag{13}$$

is the limiting current in the membrane.

The equality of the diffusional and migrational contributions to J_{TBA^+} also implies that the potential drop inside the membrane is

$$\Delta\phi_M \equiv \phi^o(d) - \phi^o(0)$$
$$= (1/f)\ln[(1 - I/I_{LM})/(1 + I/I_{LM})]$$
$$= -(2/f)\text{arctanh}(I/I_{LM}) \quad (14)$$

2.2.3. Interfacial ion transfer kinetics

The Butler–Volmer equation for the DBL/SLM interfaces at $x = 0$ and $x = d$ is [8]

$$J_{TBA^+} = k^0 c^w_{TBA^+}(0)^{(1-\alpha)} c^o_{TBA^+}(0)^{\alpha}[e^{-\alpha f\eta(0)} - e^{(1-\alpha)f\eta(0)}] \quad (15a)$$

$$J_{TBA^+} = k^0 c^w_{TBA^+}(d)^{(1-\alpha)} c^o_{TBA^+}(d)^{\alpha}[e^{-(1-\alpha)f\eta(0)} - e^{\alpha f\eta(d)}] \quad (15b)$$

where k^0 is the standard rate constant and $\eta(0)$, $\eta(d)$ are the overpotentials. When the transfer coefficient α is set equal to 1/2, Eqs. (15a)–(b) give

$$\Delta^o_w\phi(0) = \Delta^o_w\phi^0_{TBA^+} - \frac{1}{f}\left\{\ln\frac{c^o_{TBA^+}(0)}{c^w_{TBA^+}(0)} + 2\,\text{arcsinh}\frac{I}{I_k(0)}\right\} \quad (16a)$$

$$\Delta^w_o\phi(d) = \Delta^w_o\phi^0_{TBA^+} - \frac{1}{f}\left\{\ln\frac{c^w_{TBA^+}(d)}{c^o_{TBA^+}(d)} + 2\,\text{arcsinh}\frac{I}{I_k(d)}\right\} \quad (16b)$$

where

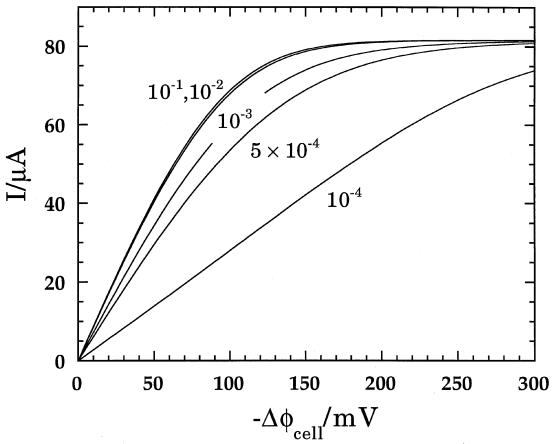

Fig. 2. Effect of the standard rate constant (shown on the curves in cm/s units) on the theoretical current-voltage curves. The following values have been used: $A = 3$ cm^2, $d = 1.1 \times 10^{-2}$ cm, $\omega = 8$ Hz, $c_s = 0.1$ M, $c_t = 0.1$ mM, $c_m = 5$ mM, $D^w_{TBA^+} = 5.13 \times 10^{-6}$ cm^2/s and $D^o_{TBA^+} = 3.72 \times 10^{-7}$ cm^2/s.

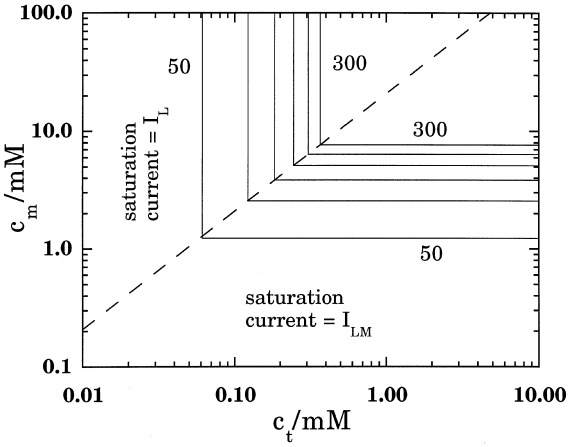

Fig. 3. Lines of equal saturation current corresponding to the values 50, 100, 150, 200, 250 and 300 μA. The points where the limiting current inside the membrane equals that in the diffusion boundary layer ($I_L = I_{LM}$) have been represented by a dashed line. Parameter values as in Fig. 2.

$$I_k(0) \equiv 2FAk^0[c^w_{TBA^+}(0)c^o_{TBA^+}(0)]^{1/2} \quad (17a)$$

and

$$I_k(d) \equiv 2FAk^0[c^w_{TBA^+}(d)c^o_{TBA^+}(d)]^{1/2} \quad (17b)$$

are the exchange currents at the DBL/SLM interfaces.

The current–voltage characteristics, in the case $c_t \ll c_s$, are finally obtained by introducing Eqs. (14) and (16a)–(b) into Eq. (6)

$$-f\Delta\phi_{cell} \approx 2\,\text{arctanh}(I/I_L) + 4\,\text{arctanh}(I/I_{LM}) + 2\,\text{arcsinh}[I/I_k(d)] + 2\,\text{arcsinh}[I/I_k(0)]. \quad (18)$$

Fig. 2 shows a calculation obtained from Eq. (18) and the following parameter values: $A = 3$ cm^2, $d = 1.1 \times 10^{-2}$ cm, $\omega = 8$ Hz, $c_s = 0.1$ M, $c_t = 0.1$ mM, $c_m = 5$ mM, $D^w_{TBA^+} = 5.13 \times 10^{-6}$ cm^2/s and $D^o_{TBA^+} = 3.72 \times 10^{-7}$ cm^2/s, where the diffusion coefficients have been taken from Ref. [9] and estimated from Walden's rule [10], respectively. This figure shows that these concentrations are suitable for the determination of rate constants of the order of 10^{-3} cm/s or smaller. A higher concentration of TBA^+ in the organic phase should be used to determine larger rate constants.

Since the tanh functions are bounded, Eq. (18) describes current–voltage curves that saturate to I_L or I_{LM}, whichever is lower (Fig. 3). In particular, a large value of c_t and a small value of c_m would certainly result in a saturation current determined by the membrane and, therefore, independent of the rotation frequency. Contrarily, when c_t is small and c_m large, the current saturates to I_L, which is frequency dependent. In these two cases, where one of the diffusional contri-

butions clearly dominates, the kinetic effects are hardly visible in the shape of the current–voltage curve and the determination of the standard rate constant might result in a wrong value. The choice of the concentrations c_t and c_m is then very important in this method.

2.3. The Koutecky–Levich plot

In the RDC system the effect of mass transfer across the DBLs can be eliminated by carrying out measurements at different rotation speeds and extrapolating to $\omega \to \infty$. In this limit, the permeability of the DBLs is so large that the TBA^+ flux is only determined by the membrane and the interfacial regions. The extrapolation procedure is often carried out by fitting the experimental data to a straight line in a Koutecky–Levich plot, i.e. in a I^{-1} versus $\omega^{-1/2}$ plot at constant $\Delta\phi_{cell}$, and the kinetic information is then obtained from the intercept. However, when the rotation frequency is increased at constant applied potential, not only δ decreases and I_L increases, but also the electric current increases, the exchange current $I_k(0)$ increases and the exchange current $I_k(d)$ decreases. As a result, the different terms on the righthand side of Eq. (18) change in such a way that *the Koutecky–Levich plot is non-linear*. The intercept obtained from the extrapolation of experimental data in a given frequency range differs then from the expected value. This fact is very important because of the limited range of frequencies available in the RDC system (typically, from 1 to 10 Hz).

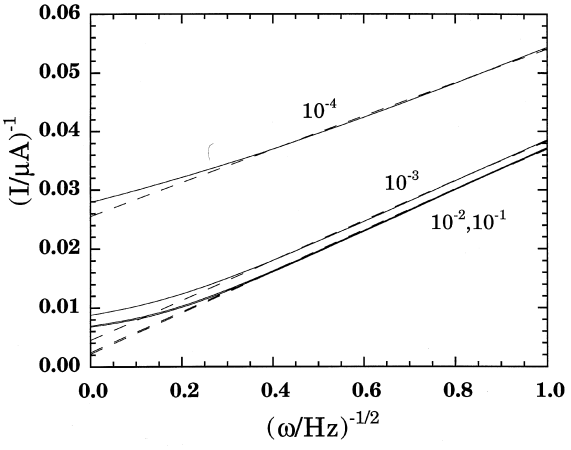

Fig. 4. Effect of the standard rate constant (shown on the curves in cm/s units) on the theoretical Koutecky–Levich plots (continuous lines). The dashed lines are linear fittings to the 1–10 Hz values. The following parameter values have been used: $-\Delta\phi_{cell} = 100$ mV and $c_m = 5$ mM. Other parameter values as in Fig. 2.

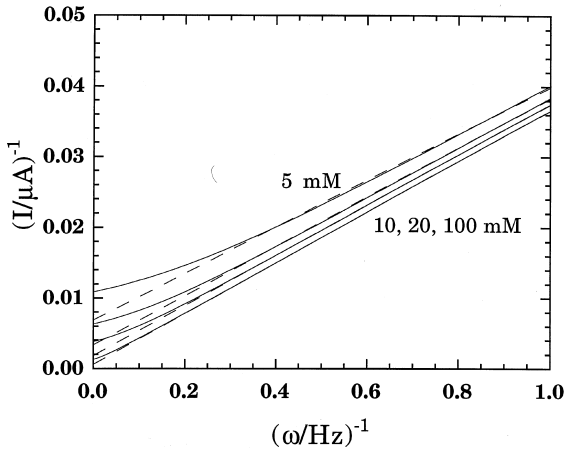

Fig. 5. Effect of the transferring ion concentration in the organic phase (c_m values shown on the curves) on the theoretical Koutecky–Levich plots (continuous lines). The dashed lines are linear fittings to the 1–10 Hz values. The following parameter values have been used: $-\Delta\phi_{cell} = 100$ mV and $k^0 = 5 \times 10^{-4}$ cm/s. Other parameter values as in Fig. 2.

Fig. 4 shows a theoretical calculation which illustrates the non-linearity of the I^{-1} versus $\omega^{-1/2}$ plots. The continuous lines represent the theoretical calculations and the dashed lines the linear fitting to the 1–10 Hz values. It is observed that the intercept of the linear fitting, $1/I_{\omega\to\infty}^{1-10\,Hz}$, significantly differs from the actual value of the reciprocal of the current in this limit, $1/I_{\omega\to\infty}$, when the standard rate constant is of the order of 10^{-3} cm/s or larger. This difference also depends on the concentration c_m of the transferring ion in the organic phase as shown in Fig. 5. In particular, it is observed that the difference between the values of $I_{\omega\to\infty}^{1-10\,Hz}$ increases with increasing c_m (note that the ordinate is the reciprocal of the current), though this difference is not important when c_m is of the order of several tens of mM or smaller (for the value $k^0 = 5 \times 10^{-4}$ cm/s here considered).

The difference between the values of $I_{\omega\to\infty}^{1-10\,Hz}$ and $I_{\omega\to\infty}$ also increases with increasing applied potential as shown in Fig. 6. This effect, together with that of c_m, is analyzed in detail in Table 1. The k^0 values that appear in the last column of Table 1 are estimations calculated from a simplified current–voltage equation based on negligible mass transfer limitations inside the membrane ($I \ll I_{LM}$), i.e.

$$I_{\omega\to\infty} = I_k \sinh(-f\Delta\phi_{cell}/4) \tag{19}$$

where

$$I_k \equiv 2FAk^0(c_t c_m)^{1/2}. \tag{20}$$

In the case $c_m = 1$ mM, the difference between the values of $I_{\omega\to\infty}^{1-10\,Hz}$ and $I_{\omega\to\infty}$ is smaller than 5% but

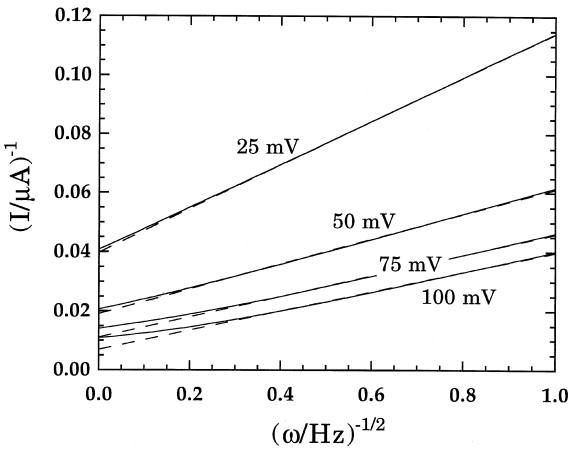

Fig. 6. Effect of the applied potential ($-\Delta\phi_{cell}$ values shown on the curves) on the theoretical Koutecky–Levich plots (continuous lines). The dashed lines are linear fittings to the 1–10 Hz values. The following parameter values have been used: $c_m = 5$ mM and $k^0 = 5 \times 10^{-4}$ cm/s. Other parameter values as in Fig. 2.

the mass transfer resistance in the organic phase represents a significant contribution to the total mass transfer resistance and ca. 35% of the applied potential drop appears inside the membrane. Under these circumstances, the use of Eq. (19) leads to k^0 estimations which are up to 75% smaller than the actual value ($k^0 = 5 \times 10^{-4}$ cm/s).

Higher values of c_m result in smaller potential drops in the organic phase but also in larger differences between $I_{\omega\to\infty}^{1-10\,Hz}$ and $I_{\omega\to\infty}$. For instance, when $c_m = 10$ mM the potential drop inside the membrane is reduced to 21% of $-\Delta\phi_{cell}$ and the difference between $I_{\omega\to\infty}^{1-10\,Hz}$ and $I_{\omega\to\infty}$ increases from 4% at $-\Delta\phi_{cell} = 25$ mV up to 90% at $-\Delta\phi_{cell} = 100$ mV. It is therefore concluded that, if a simplified equation such as Eq. (19) is to be used, the value obtained for the standard rate constant only coincides with the actual one in the limit of zero applied potential and high c_m. In practice, the highest concentration c_m to be used becomes determined by the limited solubility of the organic salt (or by the appearance of ion pairing effects if they are not taken into account in the analysis). Note, finally, that the increase in $k^0_{1-10\,Hz}$ with the applied potential that can be observed in Table 1 for the higher values of c_m is a consequence of the difference between the values of $I_{\omega\to\infty}^{1-10\,Hz}$ and $I_{\omega\to\infty}$ and could lead to overestimation of the rate constant if too high values of the applied potential were used.

A better estimation of k^0 can be obtained by extending Eq. (19) to the most common case of mixed kinetic/membrane control. The current–voltage characteristic is then given by

$$-f\Delta\phi_{cell} = 4\,\mathrm{arctanh}(I^{o}_{\omega\to\infty}/I_{LM}) + 2\,\mathrm{arcsinh}[I_{\omega\to\infty}/I_k(d)] + 2\,\mathrm{arcsinh}[I_{\omega\to\infty}/I_k(0)], \quad (21)$$

where different exchange currents $I_k(0)$ and $I_k(d)$ are used due to concentration polarization inside the membrane. Eq. (21) is a transcendental equation that can be solved for k^0 following a simple procedure. Since

Table 1. Effect of the transferring ion concentration in the organic phase and the applied potential on the standard rate constant determined from Koutecky–Levich plots. The true rate constant used in these calculations is $k^0 = 5 \times 10^{-4}$ cm/s. Other parameter values as in Fig. 2

c_m (mM)	c_t (mM)	I_{LM} (μA)	$-\Delta\phi_{cell}$ (mV)	$I_{\omega\to\infty}$ (μA)	$-\Delta\phi_M$ (mV)	$I_{\omega\to\infty}^{1-10\,Hz}$ (μA)	$k^0_{1-10\,Hz}$ (10^{-4} cm/s)
1	0.1	39.2	25	6.7	8.8	6.7	1.5
			50	13.0	17.5	13.2	1.4
			75	18.6	26.2	19.2	1.3
			100	23.3	35.0	24.7	1.2
5	0.1	195.3	25	24.5	6.4	25.1	2.5
			50	48.3	12.8	53.6	2.6
			75	71.0	19.3	90.7	2.8
			100	92.0	25.9	145.2	3.1
10	0.1	391.6	25	40.8	5.3	42.4	3.0
			50	81.2	10.7	94.8	3.2
			75	120.5	16.2	172.3	3.7
			100	158.5	21.8	299.7	4.5

$c^{o}_{TBA^+}(d) < c^{o}_{TBA^+}(0)$ (see Eq. (12)) the kinetic limitations are more likely to be observed at the $x = d$ interface. This suggests rewriting Eq. (21) in the form

$$I_k = \frac{I_{\omega\to\infty}(1 - I_{\omega\to\infty}/I_{LM})^{-1/2}}{\sinh\{-f\Delta\phi_{cell}/2 - 2\,\mathrm{arctanh}(I_{\omega\to\infty}/I_{LM}) - \mathrm{arcsinh}[I_{\omega\to\infty}(1 + I_{\omega\to\infty}/I_{LM})^{-1/2}/I_k]\}} \quad (22)$$

which can be solved iteratively from an initial guess of k^0. The accuracy of the rate constant calculation from Eq. (22) is mostly determined by the difference between the values of $I^{1-10\,Hz}_{\omega\to\infty}$ and not so much by the relative importance of mass transfer in the organic phase and interfacial transfer. That is, the problem commented in Table 1 in relation to the use of low concentrations in the organic phase is overcome by using Eq. (22).

2.4. The apparent electrical resistance at low applied potentials

Fig. 2 has shown that the rate constant can be determined from its effect on the shape of the current–voltage curves. In particular, the initial slope of these curves can be used in the determination of the standard rate constant for ion transfer. From a physical point of view, however, the reciprocal of this slope is a more convenient magnitude, for it represents the apparent electrical resistance at low applied potentials, $R_{app} \equiv -\Delta\phi_{cell}/I$. The term apparent has to be introduced here because the ion transport across this system takes place with significant concentration polarization.

At low applied potentials ($I \ll I_L$, I_{LM}, I_k), Eq. (18) simplifies to

$$R_{app} = (2RT/F)(1/I_L + 2/I_{LM} + 2/I_k). \quad (23)$$

The contribution to R_{app} from the interfacial regions is composed of the two charge transfer resistances, $2R_{ct} = 4RT/FI_k$, and the concentration polarization contribution, which can be easily estimated from the sum of the equilibrium Nernst potentials

$$\Delta^{o}_{w}\phi_{eq}(0) + \Delta^{w}_{o}\phi_{eq}(d) = -(2/f)[\mathrm{arctanh}(I/I_L) + \mathrm{arctanh}(I/I_{LM})] \quad (24)$$

as $(2RT/F)(1/I_L + 1/I_{LM})$. The other contribution to R_{app} in Eq. (23), i.e. $2RT/FI_{LM}$, is the apparent resistance of the organic phase.

Equations (18) and (23) show that the kinetic effects at the liquid/liquid interfaces lead to current–voltage curves with the same saturation value (although it might not be reached within the potential window) but different initial slopes. Then, if the values of I_L and I_{LM} are determined from the saturation currents in different experiments and the value of R_{app} is accurately known, Eq. (23) can be used to calculate k^0. It is also possible to identify the different contributions to R_{app} from their dependence on the rotation frequency and the TBA^+ concentration in the aqueous and organic phase. In particular, since Eq. (23) can be written in the form

$$R_{app} = S\omega^{-1/2} + R_{app,\omega\to\infty}, \quad (25)$$

a plot of R_{app} versus $\omega^{-1/2}$ would yield a straight line of slope $S = 1.286RTv^{1/6}/[F^2A(D^{w}_{TBA^+})^{2/3}c_t$ and intercept $R_{app,\omega\to\infty} = (4RT/F)(1/I_{LM} + 1/I_k)$. This method of analysis is essentially the same as the Koutecky–Levich method, for the Koutecky–Levich lines are drawn at constant applied potential and therefore their ordinate only differs from R_{app} in a constant factor. The difference is then in the applied potentials under consideration, which must be low enough so as to allow for the linearization of Eq. (18) into Eq. (23). That is, since concentration polarization makes the Koutecky–Levich plots non-linear, the non-linearity disappears at low applied potentials, when concentration polarization is negligible (Fig. 6).

Fig. 7 shows the dependence of R_{app} on the concentrations c_t and c_m, for the case $k^0 = 5 \times 10^{-4}$ cm/s. The determination of the standard rate constant from R_{app} will be more accurate if it is carried out when k^0 has its larger influence on R_{app}. The variation of R_{app} with c_t at constant R_{ct} (i.e. constant value of the pro-

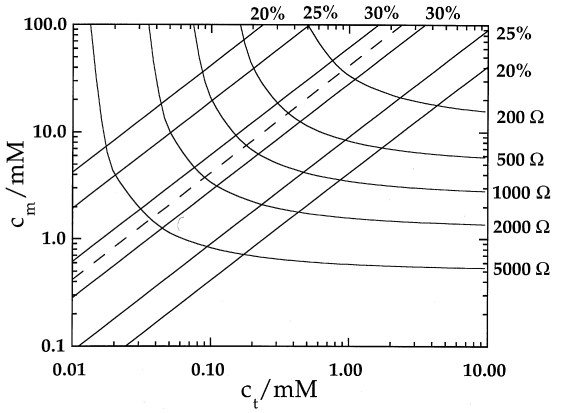

Fig. 7. Curved lines: R_{app} as a function of the concentrations c_t and c_m. Straight lines: Relative contribution of the charge transfer resistance to R_{app}. The dashed line represents the largest kinetic effects on R_{app} (i.e. $I_L = I_{LM}/2$), which in this case corresponds to 30.4%. The standard rate constant has been set equal to $k^0 = 5 \times 10^{-4}$ cm/s and the other parameter values as in Fig. 2.

duct $c_t c_m$) shows that R_{app} is minimum when $I_L = I_{LM}/2$ and then the influence of R_{ct} on R_{app} is at its largest. Fig. 7 also shows the relative contribution of R_{ct} to R_{app} in % and it is clearly seen that, for these parameter values, this relative contribution takes its larger value of ca. 30% along the line $I_L = I_{LM}/2$.

3. Experimental

TBACl (Sigma) was used as the transferring ion and LiCI (Merck, p.a.) as the supporting electrolyte in the aqueous phase (Milli-Q purified water). Tetrakis-(4-fluorophenyl)-borate ($TPBF_4^-$) was chosen as the organic anion because of its high hydrophobicity. $TBATPBF_4$ was precipitated from aqueous TBACl and $NaTPBF_4^-$ (Aldrich, 98%) and recrystallised from ethanol. 2-Nitrophenyl-octylether (Fluka, Selectophore) was used as received.

The organic phase was supported in a Durapore GVHP (pore size 0.22 μm) hydrophobic membrane. The membrane radius was 1.0 cm, its thickness 1.1×10^{-2} cm and its porosity ca. 75%. The membrane was soaked in organic solution and equilibrated overnight with the aqueous solution. The membrane was mounted onto a bevelled annulus that was then screwed to the rotating cylinder. An Oxford Electrodes rotating diffusion cell with two large area Ag/AgCl-electrodes was used. The rotation rates varied from 1 to 10 Hz.

The current–voltage curves were measured both by applying potential steps and waiting the current to reach a steady value and by imposing a slow potential sweep (1 mV/s). A comparison between the two methods (sweeps and steps) gave similar response within the experimental error. The sweep rate was experimentally chosen to yield a quasi-steady state curve. At 1 mV/s some hysteresis was observed in the voltammograms probably due to the transient behavior of the system. However, the use of slower sweep rates could not solve this problem because the long times required to run a cycle led to changes in concentrations that were again observed in the form of hysteresis. In absence of true steady-state values, the present analysis is based on the assumption that the average between the forward and backward sweeps can be considered as a quasi-steady state current–voltage curve.

Conventional cyclic voltammograms of the cell

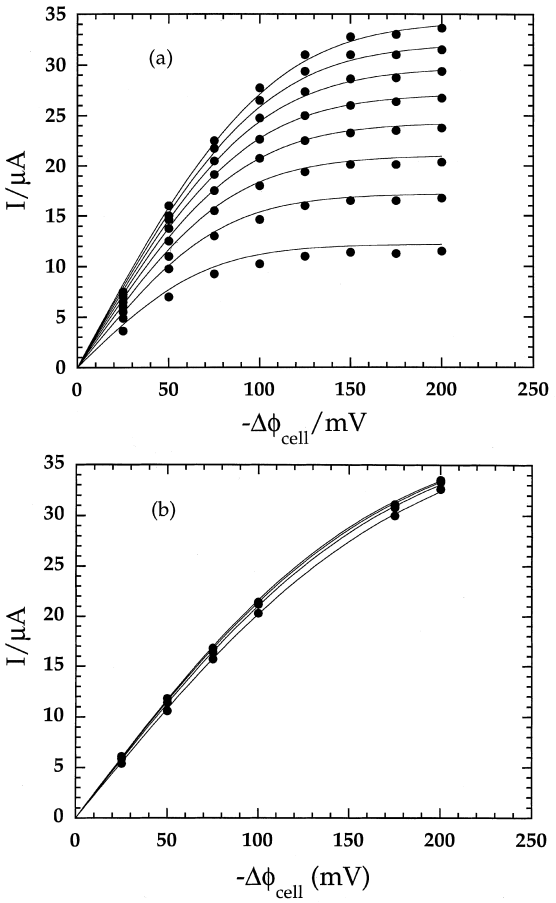

Fig. 8. Current–voltage curves for the concentrations: (a) $c_t = 0.05$ mM and $c_m = 10$ mM, and (b) $c_t = 0.2$ mM and $c_m = 2.5$ mM. The full circles show the experimental data and the lines represent the best fit to Eq. (18). The rotation frequencies (from bottom to top) are: (a) 1.00, 2.00, 3.00, 4.00, 5.00, 6.00, 7.00 and 8.00 Hz, and (b) 2.00, 4.00, 6.00 and 8.00 Hz.

were also recorded in the 4-electrode set-up usually employed in ITIES studies in order to obtain the value of $D^o_{TBA^+}$. $BTPPA^+$ is the bis(triphenylphosphoranylidene)ammonium cation and $TPBCl_4^-$ is the tetrakis(4-chlorophenyl)borate anion. A detailed description of cell and apparatus are given in Ref. [11].

	aqueous solution	organic solution	aqueous solution	
Ag/AgCl	1 mM NaCl + 1 mM NaTPB	10 mM BTPPATPBCl$_4$ + 0.5 mM TBATPBCl$_4$	10 mM LiCl	AgCl/Ag

4. Results and discussion

Fig. 8(a) and (b) show the two different types of current–voltage curves that can be observed with RDC. The saturation current in Fig. 8(a) is determined by mass transfer in the aqueous phase, and therefore shows the expected linear dependence on $\omega^{1/2}$. On the contrary, the saturation current in Fig. 8(b) is determined by mass transfer in the organic phase and turns out to be independent on the rotation frequency. From the observed values of the saturation current in Fig. 8(a) and (b), $I_L(a) = 11.9$ μA $(\omega/\text{Hz})^{1/2}$ and $I_{LM}(b) = 38$ μA, and Eqs. (11) and (13), the TBA^+ diffusion coefficient in aqueous and organic phase can be estimated as $D^w_{TBA^+} = 5.5 \times 10^{-6}$ cm^2/s and $D^o_{TBA^+} = 1.8 \times 10^{-7}$ cm^2/s, where the effective membrane area $A = 3.14 \times 0.75 = 2.36$ cm^2 has been used. These values are to be compared to $D^w_{TBA^+} = 5.13 \times 10^{-6}$ cm^2/s from Ref. [9] and $D^o_{TBA^+} = 2.7 \times 10^{-7}$ cm^2/s, which has been obtained by cyclic voltammetry and the Randles–Sevcik equation.

The apparent resistance at low potentials of the curves in Fig. 8(a) and (b) follow the relations

$$R_{app}\ (\Omega) = 6000(\omega/\text{Hz})^{-1/2} + 1020 \quad (26a)$$

and

$$R_{app}\ (\Omega) = 1500(\omega/\text{Hz})^{-1/2} + 3650, \quad (26b)$$

respectively. The slopes S are in the expected ratio $c_t(b)/c_t(a) = 4$. The frequency independent terms, $R_{app,\omega\to\infty}$, yield $I_k = 700$ μA and $I_{LM}(b) = 29.0$ μA when the ratio $I_{LM}(a)/I_{LM}(b) = c_m(a)/c_m(b) = 4$ is imposed. This value of the exchange current allows for a first estimation of the rate constant for ion transfer, $k^0 = 2.2 \times 10^{-3}$ cm/s. However, it can be easily seen from Fig. 8(b) that the value $I_{LM}(b) = 29.0$ μA is not consistent with the observed currents (in fact, $I_{LM}(b)$ was estimated as 38 μA in the previous paragraph). Similarly, the slope in Eq. (26a) leads to $I_L(a) = (2RT/FS)\omega^{1/2} = 8.5$ μA $(\omega/\text{Hz})^{1/2}$, which is not in agreement with the observed currents in Fig. 8(a). These inconsistencies might be due to the inaccuracy of the R_{app} values, which have been calculated from a linear fit with zero intercept to the 25 and 50 mV data. This procedure has been chosen to reduce the influence of random deviations in the experimental data, while still using low enough applied potentials for the linearization involved in Eq. (23) to be valid.

Alternatively, the data in Fig. 8(a) and (b) can be analyzed by means of Koutecky–Levich plots. In particular, the data corresponding to 25, 50 and 100 mV of applied potential yield

$$(I/\mu A)^{-1} = 0.219(\omega/\text{Hz})^{-1/2} + 0.055 \quad (27a)$$

$$(I/\mu A)^{-1} = 0.123(\omega/\text{Hz})^{-1/2} + 0.0187 \quad (28a)$$

$$(I/\mu A)^{-1} = 0.0955(\omega/\text{Hz})^{-1/2} + 0.0013 \quad (29a)$$

in the case of Fig. 8(a) and

$$(I/\mu A)^{-1} = 0.064(\omega/\text{Hz})^{-1/2} + 0.139 \quad (27b)$$

$$(I/\mu A)^{-1} = 0.029(\omega/\text{Hz})^{-1/2} + 0.0737 \quad (28b)$$

$$(I/\mu A)^{-1} = 0.0076(\omega/\text{Hz})^{-1/2} + 0.0438 \quad (29b)$$

in the case of Fig. 8(b). The intercepts in Eqs. (27a)–(b), (28a)–(b) and (29a)–(b) can be conveniently analysed with the help of Eq. (22), although only the 25 mV data is reliable because the difference between $1/I^{1-10\ Hz}_{\omega\to\infty}$ and $1/I_{\omega\to\infty}$ is maybe too large for higher applied potentials. Thus, by using $I_{LM}(a) = 4 \times I_{LM}(b) = 152$ μA (as estimated directly from Fig. 8(b)), Eqs. (27a) and (28a) yield the values $I_k = 145$ μA and $I_k = 452$ μA, respectively, while Eq. (29a) cannot be used because the extrapolated value of $1/I^{1-10\ Hz}_{\omega\to\infty}$ is too small. Analogously, the values of $1/I^{1-10\ Hz}_{\omega\to\infty}$ from Eqs. (27b), (28b) and (29b) yield $I_k = 135$, 121 and 92 μA, respectively, when $I_{LM}(b) = 38$ μA is used in Eq. (22). However, these values are rather inaccurate because they are very sensitive to $1/I_{\omega\to\infty}$ and $I_{LM}(b)$ and these magnitudes have not been accurately determined. The estimation of the rate constant must then be obtained from the value $I_k = 145$ μA and yields $k^0 = 4.5 \times 10^{-4}$ cm/s.

Since the above values of the exchange current I_k have been obtained from the nonlinearized Eq. (22),

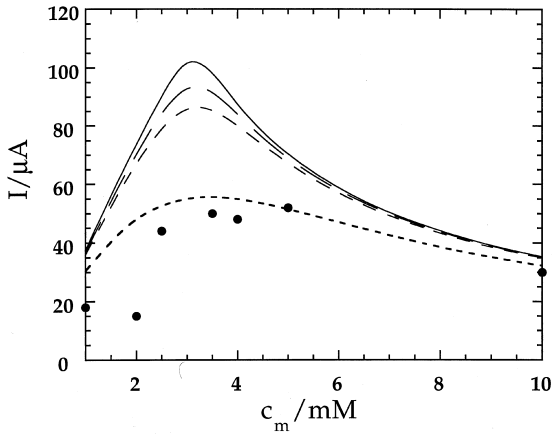

Fig. 9. The full circles show the current observed at 200 mV applied potential and 6 Hz in different systems with $c_m c_t = 0.5$ mM^2. The lines have been calculated from equation (18) with $A = 3$ cm^2, $d = 1.1 \times 10^{-2}$ cm, $D^w_{TBA^+} = 5.13 \times 10^{-6}$ cm^2/s and $D^o_{TBA^+} = 3.72 \times 10^{-7}$ cm^2/s. The rate constant values used in the calculations are: (———) ∞, (— — —) 10^{-3} cm/s, (— – —) 5×10^{-4} cm/s and (- - -) 10^{-4} cm/s.

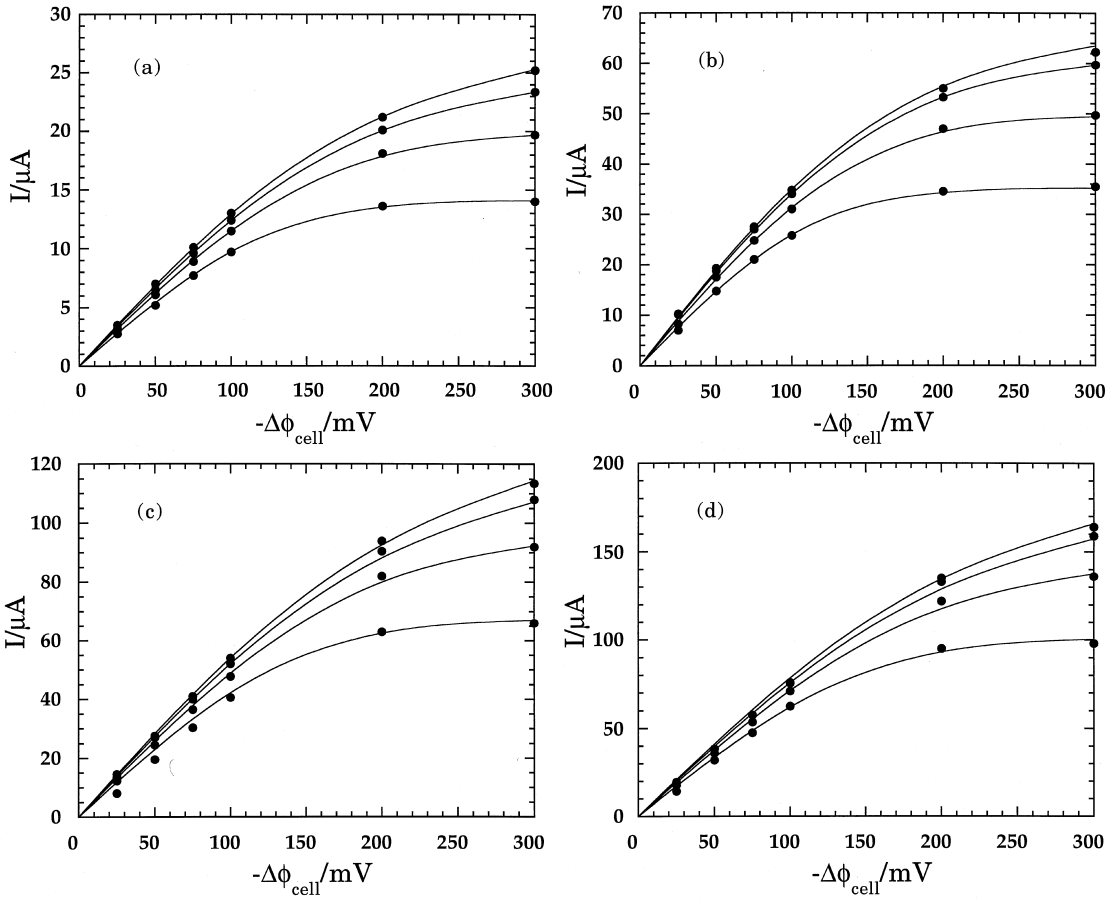

Fig. 10. Current–voltage curves for the concentrations: (a) $c_t = 0.04$ mM and $c_m = 2$ mM, (b) $c_t = 0.1$ mM and $c_m = 5$ mM, (c) $c_t = 0.2$ mM and $c_m = 10$ mM and (d) $c_t = 0.3$ mM and $c_m = 15$ mM. The full circles show the experimental data and the lines represent the best fit to Eq. (18). The rotation frequencies (from bottom to top) are 2.00, 4.00, 6.00 and 8.00 Hz.

they can be used to check the validity of linearized equations such as Eq. (23). It turns out that the linearization is valid for the 25 mV data and underestimates the exchange current in about 15% for the 50 mV data. The above procedure to obtained the R_{app} values to be used in Eq. (23) seems then to be justified.

Finally, the experimental data can also be analysed by means of non-linear fitting to Eq. (18) with three parameters related to the ion transfer across the aqueous, interfacial and organic phases. These fitting parameters contain the membrane area A as a proportionality factor. However, if A is estimated as the effective area (2.36 cm^2), the fitting parameters can be identified with $D^w_{TBA^+}$, $D^o_{TBA^+}$ and k^0. This is the procedure followed here, with the understanding that the value of A can indeed vary for the different membrane samples used in every run and this can introduce errors of the order of 10% in the values of the fitting parameters. In the case of Fig. 8(a) and (b), this procedure yields $D^w_{TBA^+} = 5.9 \times 10^{-6}$ cm^2/s, $D^o_{TBA^+} = 1.8 \times 10^{-7}$ cm^2/s and $k^0 = 3.3 \times 10^{-4}$ cm/s. This low value of the rate constant is thought to be related to the fact that the observed values of the initial slope in the current–voltage curves and the saturation current do not follow the simple relation given by Eq. (23). When fitting the experimental data to Eq. (18) this disagreement can be masked by an unrealistically small value of the rate constant, which reduces the initial slopes while leaving unchanged the saturation current.

As a conclusion of this preliminary analysis of the experimental data, it is proposed to consider different sets of experimental data and study the saturation current $I_L = C\omega^{1/2}$, where C is a constant determined from the non-linear fit of the current–voltage curves to Eq. (18), the slope S and the intercept $R_{app,\omega \to \infty}$ in the linear fit of R_{app} against $\omega^{-1/2}$ and the Koutecky–Levich plot corresponding to 25 mV. Systems where the saturation current is I_{LM} yields more inaccurate values and, therefore, not considered in the following analysis.

Table 2. Limiting currents and apparent electrical resistance at low potentials corresponding to Fig. 10

c_m (mM)	c_t (mM)	C (μA Hz$^{-1/2}$)	I_{LM} (μA)	k^0 (10^{-4} cm/s)	S (Ω Hz$^{1/2}$)	$R_{app,\omega\to\infty}$ (Ω)
2	0.04	10.0	28.7	4.4	6448	4959
5	0.1	25.0	75.6	6.6	2790	1502
10	0.2	47.9	134.6	2.6	1695	1185
15	0.3	71.9	202.2	2.2	892	958

In order to obtain the best possible value for k^0 it is important to consider those sets of experimental data where the kinetic effects are important. According to Fig. 7, this is best achieved when $I_L = I_{LM}/2$. Information on the location of the line $I_L = I_{LM}/2$ in the concentrations plane $c_t - c_m$ is then required. Fig. 9 shows the observed current at 200 mV and 6 Hz for different experiments where the product of concentrations was kept constant to $c_t c_m = 0.5$ mM^2. Equation (18) predicts that this data should have a maximum when $I_L = I_{LM}$ and that the maximum should be relatively sharp in absence of kinetic effects and rather flat in their presence. The experimental data show a maximum around 4 mM which does not seem to be very sharp. Hence, the line $I_L = I_{LM}$ corresponds to $c_m/c_t = c_m^2/c_m c_t = 16/0.5 \approx 30$ and the line $I_L = I_{LM}/2$ must correspond to $c_m = 60 c_t$. Note that the horizontal shift observed in Fig. 9 between the position of the maxima in the theoretical curves and the position of the experimental maximum simply indicates that the actual ratio $D^w_{TBA^+}/D^o_{TBA^+}$ is larger than that used in the theoretical calculations ($D^w_{TBA^+} D^o_{TBA^+} = 13.8$ as estimated from Walden's rule).

Fig. 10 shows the current–voltage curves of four systems with concentrations along the line $c_m \approx 50 c_t$: (a) $c_t = 0.04$ mM and $c_m = 2$ mM, (b) $c_t = 0.1$ mM and $c_m = 5$ mM, (c) $c_t = 0.2$ mM and $c_m = 10$ mM and (d) $c_t = 0.3$ mM and $c_m = 15$ mM. The full circles represent the experimental data, while the lines show the best fit to Eq. (18). The data in Fig. 10(a)–(d) were fitted independently to Eq. (18), i.e. with three free parameters for each one of the four data sets. These three parameters can be considered to be C, I_{LM} and k^0 and their values are shown in Table 2. In spite of the good agreement between the theoretical predictions and the experimental data, the fitted value of the rate constant is considered to be unrealistically small for the reasons commented above. This fitting procedure, however, proves to be useful in the determination of the constant C in the relation $I_L = C\omega^{-1/2}$. Table 2 also shows the slope S and the intercept $R_{app,\omega\to\infty}$ in the linear fit of R_{app} against $\omega^{-1/2}$. The exchange current I_k can be calculated from the data in Table 2 by making use of the relation

$$\frac{1}{I_k} = \frac{R_{app,\omega\to\infty}}{2CS} - \frac{1}{I_{LM}}, \tag{30}$$

which yields $k^0 = 2.1 \times 10^{-3}$ cm/s for $c_m = 2$ mM and $k^0 = 4.1 \times 10^{-4}$ cm/s for $c_m = 15$ mM. In the other two cases, $c_m = 5$ mM and $c_m = 10$ mM, the output for I_k is negative, meaning that the effect of the interfacial ion transfer is of the same order of magnitude than the experimental uncertainties.

It is interesting to note from Table 2 that there is clear deviation from the expected proportionality between I_{LM} and c_m. Even though the fitted values of I_{LM} are rather uncertain because their influence in the shape of the current–voltage curves can be masked by the value of k^0, it seems apparent that ion pairing in the bulk of the organic phase is important even for these low concentrations. A rough estimation from the data in Table 2 shows that the dissociation degree could be of the order of 90% when $c_m = 15$ mM. Other estimations based on fittings to a modified Eq. (18) taking into account bulk ion pairing, yielded smaller dissociation degrees. In any case, since nominal concentrations are used to calculate the rate constant k^0 from the exchange current I_k, it can be concluded that bulk ion pairing has an influence leading to underestimation of k^0. The value $k^0 = 4.1 \times 10^{-4}$ cm/s

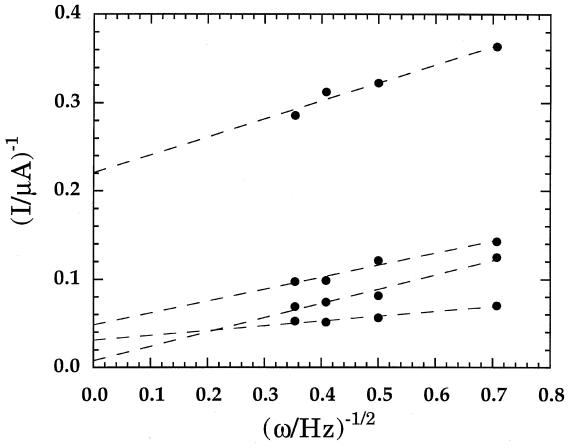

Fig. 11. Experimental Koutecky–Levich plots corresponding to the $-\Delta\phi_{cell} = 25$ mV data (full circles) in Fig. 10(a)–(d). The dashed lines are linear fittings to the experimental data. The concentrations increase from top (data from Fig. 10(a)) to bottom (data from Fig. 10(d)).

obtained above from $c_m = 15$ mM underestimates then the actual value due to ion pairing.

Fig. 11 shows the Koutecky–Levich plots corresponding to the 25 mV data in Fig. 10. From the extrapolated values $I_{\omega\to\infty}^{1-10\,\mathrm{Hz}}$, the I_{LM} values in Table 2 and Eq. (22), it is obtained that the $k^0 = 4.1\times10^{-4}$ cm/s for $c_m = 2$ mM and $k^0 = 4.0\times10^{-4}$ cm/s for $c_m = 15$ mM. No k^0 value could be estimated from the $c_m = 5$ mM and $c_m = 10$ mM data. As previously commented at the beginning of this section, there are certain points of disagreement between the experimental data and the theory. The most important refers to the fact that the simple theoretical relation $CS = 2RT/F$ does not hold exactly. On the contrary, the CS values calculated from Table 2 are from 1.3 to 1.6 times larger than $2RT/F$. The use of the theoretical Eq. (30) takes this into account and is believed to lead to the best estimations of k^0. However, the straightforward analysis of the experimental data using Koutecky–Levich plots and Eq. (22) seems to be affected by this disagreement and it is therefore less reliable.

Note finally that the theory presented above implicitly assumes that the potential drop from the outer boundary of the DBLs to the electrodes are negligible. Since the aqueous phases contain a high concentration of supporting electrolyte, this hypothesis seems to be justified, but still the electrical resistance of these regions has been estimated of the order of 60 Ω. This can be of the same order of magnitude than the charge transfer resistance for the larger concentrations here considered and, therefore, it seems possible that this resistance could affect the estimation of the rate constant. However, the most reliable values of the rate constant have been deduced from low concentration data and this 60 Ω electrical resistance is then clearly negligible.

5. Conclusions

The rotating diffusion cell has been thoroughly considered as a novel experimental method to study ion transfer kinetics. Similarly to the use of rotating disk electrodes [7], the use of the RDC has some experimental limitations which make it suitable for the determination of only a limited range of standard rate constant values. However, the possibility of controlling not only the applied potential and the rotation frequency but also the transferring ion concentrations in the aqueous and organic phases widens considerably this range. Furthermore, the RDC set-up yields additional information on the diffusion coefficients in the aqueous and organic phases.

Experimental conditions must be carefully chosen. In particular, the anion of the organic salt must be sufficiently hydrophobic to avoid the leakage of this salt to the aqueous phases and the transferring ion concentration in the aqueous phase must be low because the transport of this ion to the membrane must take place by convective diffusion and not by migration [7]. At the same time, this concentration must be high enough to make negligible the changes in bulk concentration during the time of the experiments.

The analysis of the experimental data is more complicated than in the case of rotating disk electrodes, as should be expected from the fact that two interfaces and three bulk phases are involved. In particular, the classical Koutecky–Levich plot provides here a value of the current that does not incorporate the effect of mass transfer in the aqueous phases, but still incorporates that of mass transfer inside the membrane and across the two interfacial regions. The rate constant can then be easily determined from this plot in the case of high concentrations of the transferring ion in the organic phase and low applied potentials by using Eq. (19). However, ion pairing effects may appear if this concentration is too high. The use of Eq. (22), though slightly more cumbersome, allows for the standard rate constant determination when smaller concentrations are used in the organic phase.

Alternatively the experimental data can be analyzed in the form of current–voltage curves by multiparametric non-linear fitting to Eq. (18). In this paper, a FORTRAN program has been employed for the fittings, although spreadsheet software could also be used. However, the appearance in Eq. (18) of mathematical functions that may diverge make it convenient to consider the applied potential as the independent variable, and hence the use of the FORTRAN program. Eq. (18) becomes a transcendental equation that must be solved to obtain the current for every value of the applied potential. This method yields the best results when several data sets corresponding to different concentrations are fitted simultaneously, but it cannot be used to estimate the rate constant when clear disagreement between the dependence of the initial slope and the saturation current on the rotation frequency is observed.

To increase the reliability of the rate constant determination, the analysis of the experimental data must be carried out taking into account the behavior of both, the initial slope and the saturation current, and hence Eq. (30) seems to be a good choice. This method has yielded the value 2×10^{-3} cm/s for the rate constant of TBA^+ ion transfer in the water/o-NPOE system, which probably underestimates the actual value.

In conclusion, the RDC is a new method that can be used to study the kinetics of ion transfer at liquid/liquid systems and work is continuing to broaden its applicability to quantitative studies.

Acknowledgements

Financial support from the European Union through project No. FMRX-CT96-0078 is acknowledged. R.L. and J.A.M. also thank the Neste Foundation for their financial support.

Appendix A

In the case $c_t \lesssim c_s$, the potential drops and the concentrations at the external membrane boundaries are obtained as follows. The local electroneutrality assumption ($c_{TBA^+} = c_{Cl^-} - c_{Li^+}$) allows writing of the TBA^+ flux as

$$J_{TBA^+} = -D^w_{TBA^+}\left[\frac{dc_{Cl^-}}{dx} - \frac{dc_{Li^+}}{dx} + f(c_{Cl^-} - c_{Li^+})\frac{d\phi}{dx}\right] \quad (A.1)$$

or simply

$$J_{TBA^+} = -2D^w_{TBA^+}\frac{dc_{Cl^-}}{dx} \quad (A.2)$$

where the zero flux density condition for Cl^- and Li^+ ions has been used. Eq. (A.2) implies that the concentration profile of the Cl^- ions is linear and varies inside the inner DBL from $(c_s + c_t)$ at $x = -\delta$ to

$$c^w_{Cl^-}(0) = (c_s + c_t)(1 - I/I_{L,Cl^-}), \quad (A.3)$$

where

$$I_{L,Cl^-} \equiv 2FAD^w_{TBA^+}(c_s + c_t)/\delta \quad (A.4)$$

is the limiting current for chloride ions. The potential drop in this DBL can thus be obtained as

$$\Delta\phi_I \equiv \phi^w(0) - \phi(-\delta) = (1/f)\ln[c^w_{Cl^-}(0)/c_{Cl^-}(-\delta)] = (1/f)\ln(1 - I/I_{L,Cl^-}). \quad (A.5)$$

In order to evaluate the TBA^+ concentration in the aqueous side of the inner DBL/SLM interface, it can be employed that

$$c_{Cl^-}(x)c_{Li^+}(x) = (c_s + c_t)c_s, \quad 0 \le x < d \quad (A.6)$$

because these two ions are not transferring and follow the Boltzmann law [12]. The local electroneutrality assumption then leads to

$$c^w_{TBA^+}(0) = (c_s + c_t)(1 - I/I_{L,Cl^-}) - c_s/(1 - I/I_{L,Cl^-}). \quad (A.7)$$

It must be observed that $c^w_{TBA^+}(0)$ is zero when I reaches

$$I_{L,TBA^+} = I_{L,Cl^-}\{1 - [c_s/(c_s + c_t)]^{1/2}\} \quad (A.8)$$

which represents the limiting current for the transferring ion and takes into account the presence of a finite amount of supporting electrolyte. That is, I_{L,TBA^+} reduces to I_L (Eq. (11)) when $c_t \ll c_s$. Eq. (A.8) also shows that, since $I_{L,TBA^+} < I_{L,Cl^-}$ the Cl^- ion does not polarize as much as TBA^+ ion.

A similar study of the outer DBL leads to

$$\Delta\phi_O \equiv \phi(d + \delta) - \phi^w(d) = -(1/f)\ln(1 + I/I_{L,Cl^-}) \quad (A.9)$$

$$c^w_{TBA^+}(d) = (c_s + c_t)(1 + I/I_{L,Cl^-}) - c_s/(1 + I/I_{L,Cl^-}). \quad (A.10)$$

References

[1] Z. Samec, T. Kakiuchi, in: H. Gerischer, C.W. Tobias (Eds.), Advances in Electrochemical Engineering, vol. 4, VCH, Weinheim, Germany, 1995.
[2] H.H. Girault, in: J.O'M. Bockris (Ed.), Modern Aspects of Electrochemistry, No. 25, Plenum Press, New York, 1993.
[3] K. Kontturi, J.A. Manzanares, L. Murtomäki, Electrochim. Acta 40 (1995) 2979.
[4] P.D. Beattie, A. Delay, H.H.J. Girault, Electrochim. Acta 40 (1995) 2961.
[5] V.J. Cunnane, D.J. Schiffrin, D.E. Williams, Electrochim. Acta 40 (1995) 2943.
[6] W.J. Albery, J.F. Burke, E.B. Leffler, J. Hadgraft, J. Chem. Soc. Faraday Trans. I 72 (1976) 1618.
[7] Yu.V. Pleskov, V.Yu. Filinovskii, The Rotating Disk Electrode, Consultants Bureau, New York, 1976.
[8] H.H.J. Girault, D.J. Schiffrin, in: A.J. Bard (Ed.), Electroanalytical Chemistry. vol. 15, Marcel Dekker, New York, 1989, p. 72.
[9] B. Hundhammer, C. Müller, T. Solomon, H. Alemu, H. Hassen, J. Electroanal. Chem. 319 (1991) 125.
[10] R.A. Robinson, R.H. Stokes, Electrolyte Solutions, Butterworths, London, 1955.
[11] A.K. Kontturi, K. Kontturi, L. Murtomäki, D.J. Schiffrin, J. Chem. Soc. Faraday Trans. 86 (1990) 931.
[12] O. Sten-Knudsen, in: D.C. Tosteson (Ed.), Membrane Transport in Biology, vol. 1, Springer-Verlag, Berlin, 1978.